HHS Public Access

Author manuscript

Am J Ophthalmol. Author manuscript; available in PMC 2017 September 13.

Published in final edited form as:

Am J Ophthalmol. 2014 May ; 157(5): 1022–1032. doi:10.1016/j.ajo.2014.02.008.

Evaluation of Retinal and Choroidal Thickness by Swept-Source Optical Coherence Tomography: Repeatability and Assessment of Artifacts

Kaweh Mansouri,
Glaucoma Sector, Department of Ophthalmology, Geneva University Hospitals, Geneva, Switzerland

Hamilton Glaucoma Center and Department of Ophthalmology, University of California, San Diego, La Jolla, California

Felipe A. Medeiros,
Hamilton Glaucoma Center and Department of Ophthalmology, University of California, San Diego, La Jolla, California

Andrew J. Tatham,
Hamilton Glaucoma Center and Department of Ophthalmology, University of California, San Diego, La Jolla, California

Nicholas Marchase, and
Hamilton Glaucoma Center and Department of Ophthalmology, University of California, San Diego, La Jolla, California

Robert N. Weinreb
Hamilton Glaucoma Center and Department of Ophthalmology, University of California, San Diego, La Jolla, California

Abstract

PURPOSE—To determine the repeatability of automated retinal and choroidal thickness measurements with swept-source optical coherence tomography (SS OCT) and the frequency and type of scan artifacts.

DESIGN—Prospective evaluation of new diagnostic technology.

METHODS—Thirty healthy subjects were recruited prospectively and underwent imaging with a prototype SS OCT instrument. Undilated scans of 54 eyes of 27 subjects (mean age, 35.1 ± 9.3 years) were obtained. Each subject had 4 SS OCT protocols repeated 3 times: 3-dimensional (3D) 6 × 6-mm raster scan of the optic disc and macula, radial, and line scan. Automated measurements

Kaweh Mansouri, Glaucoma Sector, Department of Ophthalmology, Geneva University Hospitals, Geneva, Switzerland; kawehm@yahoo.com.

Supplemental Material available at AJO.com.

ALL AUTHORS HAVE COMPLETED AND SUBMITTED THE ICMJE FORM FOR DISCLOSURE OF POTENTIAL CONFLICTS OF INTEREST and the following were reported.

were obtained through segmentation software. Interscan repeatability was assessed by intraclass correlation coefficients (ICCs).

RESULTS—ICCs for choroidal measurements were 0.92, 0.98, 0.80, and 0.91, respectively, for 3D macula, 3D optic disc, radial, and line scans. ICCs for retinal measurements were 0.39, 0.49, 0.71, and 0.69, respectively. Artifacts were present in up to 9% scans. Signal loss because of blinking was the most common artifact on 3D scans (optic disc scan, 7%; macula scan, 9%), whereas segmentation failure occurred in 4% of radial and 3% of line scans. When scans with image artifacts were excluded, ICCs for choroidal thickness increased to 0.95, 0.99, 0.87, and 0.93 for 3D macula, 3D optic disc, radial, and line scans, respectively. ICCs for retinal thickness increased to 0.88, 0.83, 0.89, and 0.76, respectively.

CONCLUSIONS—Improved repeatability of automated choroidal and retinal thickness measurements was found with the SS OCT after correction of scan artifacts. Recognition of scan artifacts is important for correct interpretation of SS OCT measurements.

THE INTRODUCTION OF OPTICAL COHERENCE TOmography (OCT) approximately 2 decades ago has contributed to better understanding and management of glaucoma.[1,2] In recent years, OCT technology has undergone several iterations with the incorporation of spectral-domain (SD) imaging that offers significant advantages over the earlier time-domain techniques.[3] These advances have led to considerable improvements in the ability to visualize individual layers of the retina in near-histologic detail,[4,5] whereas deeper ocular structures such as the choroid have remained difficult to image.

The choroid, a heavily vascularized tissue between the retina and sclera, plays a central role in ocular metabolism, volume regulation, and temperature control. Abnormalities of the choroid have been implicated in major ophthalmic conditions, most importantly in the pathophysiologic features of retinal disease.[6,7] Changes in choroidal structure[8–10] and function[11,12] also have been hypothesized to contribute to optic nerve damage in glaucoma. Until recently, postmortem histologic studies[9,11] and ultrasonography[13] were the major source of knowledge on choroidal anatomy and physiology. An important source for uncertainty about the cause-and-effect relationship of choroidal changes and disease processes arises from the lack of precision and effect of artifacts on these methods.[4]

The introduction of enhanced depth imaging (EDI) protocols,[7,14] in which an inverted image is obtained by closer placement of the SD OCT instrument to the eye, has reduced scattering effects and depth-dependent reduction in sensitivity. However in EDI OCT, improved choroidal visualization is achieved at the expense of reduced resolution of retinal layers.[14,15]

Recently, a new generation of high-penetration OCTs has been introduced that may have the potential to improve the understanding of the choroid further.[16] These swept-source (SS) OCTs use a long-wavelength light source of 1050 nm and a tunable laser, the wavelength of which can be altered in a controlled manner.[17] SS OCT systems have the potential for superior and simultaneous imaging of the retina and choroid because of the longer wavelength, potentially higher detection efficiency, and lower dispersion.[18] In the absence of automated segmentation software for SS OCT systems, previous investigators[16,19–21] have used manual (mostly single-point) measurement techniques using in-built calibers or

modification of retinal segmentation lines[22] to evaluate choroidal thickness. Given the high anatomic variability of the choroid, these are impractical for clinical use, are highly dependent on location of measurement, and may be subject to further operator effects. We recently described the use of automated segmentation for choroidal measurements using SS OCT.[17]

Before a new device can be accepted for use in clinical practice, its repeatability should be evaluated. Estimating repeatability is a prerequisite for quantifying an instrument's ability to separate real change from noise, as in the monitoring of response to treatment in retinal conditions and progression in glaucoma. Studies evaluating the repeatability and reproducibility of choroidal measurements with SS OCT in healthy Japanese subjects have used different image acquisition protocols and manual segmentation techniques, which may explain notable disparities between choroidal thickness measurements among them.[16,19–21,23–25] Artifacts represent another major concern for every imaging technique. However, none of these studies have reported the frequency and effect of image artifacts on SS OCT measurements.

The aim of the current study was to evaluate the repeatability of measurements of retinal and choroidal thickness using a prototype SS OCT instrument in healthy participants. For this purpose, built-in automated segmentation of choroidal borders was applied to 4 different image acquisition protocols. In addition, we sought to study the effect of image artifacts on SS OCT measurements.

METHODS

THIS PROSPECTIVE STUDY WAS COMPLIANT WITH HEALTH Insurance Portability and Accountability Act regulations and adhered to the Declaration of Helsinki and all federal or state laws. It was approved by the University of California, San Diego, Human Research Protections Program (institutional review board protocol no. 111356). This study was registered at http://clinicaltrials.gov (identification no. NCT01507584). Written informed consent was obtained from all participating subjects.

SUBJECTS

Thirty healthy subjects were recruited from among university employees and their families at the Shiley Eye Center, University of California, San Diego. Subjects with current ocular disease, previous ocular surgery, myopia of more than 5 diopters, or hyperopia of more than 3 diopters were excluded. All subjects had normal visual field testing results (using Statpac II, Swedish interactive thresholding algorithm 24-2, Zeiss-Humphrey Field Analyzer; Carl Zeiss Meditec, Inc, Dublin, California, USA), an IOP of 21 mmHg or less on Goldmann applanation tonometry, and no clinical signs of eye disease on slit-lamp anterior segment and fundus examination.

SWEPT-SOURCE OPTICAL COHERENCE TOMOGRAPHY

Images of the optic disc and the macular region were obtained using a prototype SS OCT system (Topcon, Inc, Tokyo, Japan). The SS OCT has an acquisition rate of 100,000 A-scans per second operated at the 1-μm wavelength region. This instrument uses a wavelength-

sweeping laser with a tuning range of approximately 100 nm as light source and has a center wavelength of 1050 nm, yielding an 8-μm axial resolution in tissue. These features allow penetration of deeper tissue through the retinal pigment epithelium into the choroid. The device has been described in more detail elsewhere.[17,26]

Four different scan protocols were used for evaluation of choroidal thickness. First, a 3-dimensional (3D) imaging data set was acquired with a 6 × 6-mm raster scan centered on the optic disc (optic disc protocol) composed of 256 B-scans, each consisting of 256 A-scans (total, 65,536 axial scans/volume) with an acquisition time of approximately 0.66 seconds. The resulting scan provides a 3D image of the optic disc and surrounding area. Second, the same 3D imaging data set was obtained covering an area of 6 × 6-mm centered on the fovea (macula protocol). Third, a radial scan protocol centered on the optic disc (12 lines, each composed of 32 B-scans, with each B-scan composed of 1024 A-scans) with an acquisition time of 4 seconds was obtained (Supplemental Figure 1, available at AJO.com). Fourth, a 12-mm horizontal line scan protocol, centered between the optic disc and the fovea and composed of 1024 A-scans for each of 96 B-scans, was obtained (acquisition time, 1 second; Supplemental Figure 2, available at AJO.com).

All scan protocols were acquired in the described order. Each scan protocol was repeated 3 times consecutively on the same visit. Participant and device were repositioned after each scan. The choroidal reference position was used for all scans. The centering of scans was achieved by internal fixation and confirmed by a fundus camera integrated in the instrument. Two experienced examiners (A.J.T., N.M.) scanned all participants. Measurements of both eyes of each study participant were obtained through undilated pupils. To be included in the analysis, all images had to have an image quality score of 45 (of 160) or more, according to manufacturer recommendation. The detailed image quality calculation is generated by a proprietary algorithm that produces an image quality score in the range of 0 to 160, which corresponds to an estimate of the signal-to-noise ratio specifically for the retinal signal. A score of 160 indicates that the all-retinal signal is of greater intensity than the estimated background, whereas a score of 0 indicates that the all-retinal signal is indistinguishable from the estimated background signal. In a 3D scan, only a single score is assigned, representing the average of all individual frames' image quality scores.

CLASSIFICATION OF ARTIFACTS

The following sources of artifacts were defined: motion artifact, signal loss resulting from blinking, and segmentation failure.[27] Quality assurance checks were carried out at the conclusion of the study by an independent grader not involved in the image acquisition process. The number of scans with an artifact, the type of the artifact, and whether the artifact affected the calculated retinal and choroidal measurements were recorded.

Motion artifacts were defined as displacement of major retinal vessels by more than 1 vessel diameter (Figure 1). Scans with blink-related signal losses were excluded automatically from the averaging process for the line scan and radial scan protocols. Information on the averaging success is available during image acquisition. In the present study, only images with a minimum 50% averaging success were considered good quality and were saved during acquisition. The used averaging technique relies on correlation statistics to determine

whether to accept a newly registered image into the composite average image. A registration operation that results in a relatively low interimage correlation is rejected, and those poorly matched image frames are not accepted into the final composite average. The displayed success rate information serves as an indication of the number of the number of frames that were included in the final composite average image. With the 3D scan protocols, blink-related signal loss is not readily visible during image acquisition (Figure 2). Therefore, postacquisition quality controls were performed, and scans with a signal loss of more than 10% (by manual measurement) of the scan area were excluded from the analysis. Failure of a segmentation line was defined when corroboration with visual inspection differed in more than 25% of the 2D scan area (3D scan protocol), in more than 25% of the scan area in more than 25% of scan lines (eg, fewer than 3 lines, radial scan protocol), and in more than 25% of the line area (line scan protocol; Figure 3). These cutoffs were chosen arbitrarily; however, other investigators have used similar cutoffs (eg, 85% concordance between manual and automated identification of posterior surface).[28] Post hoc analysis was conducted to evaluate whether reproducibility results changed significantly when all scans with the presence of blink artifacts (including less than 10%) were excluded.

CHOROIDAL AND RETINAL THICKNESS MEASUREMENT

Segmentation data were produced using the SS OCT segmentation software (version 1.43) and exported using the manufacturer's OCT batch (version 4.3.0.118) utility. The resulting data files consisted of the boundary depth information for 9 layers for each A-scan, with the values for each B-scan in a separate file. A script was developed that combined the B-scans of each examination into a single thickness file—converted from pixel space to micrometers—and, using the boundary depth of the first layer, computed the depth thicknesses of each subsequent layer for each B-scan. The thickness information then was processed using MATLAB (version 2012a; MathWorks, Inc, Natick, Massachusetts, USA) to compute the average thickness for each B-scan. Additionally, for each radial scan, the average thickness over all 12 B-scans was calculated for each layer. For each 3D scan, the average thickness and the total volume over the entire scan area was calculated for each layer. The SS OCT segmentation software outputs 0 for the boundary depths when scanning over the optic disc. We used this information to exclude the optic disc region in the average thickness calculations. Automated measurements of choroidal thickness and choroidal volume thus were obtained for all subjects. Supplemental Figure 3 (available at AJO.com) demonstrates segmentation of retina and choroid at the optic disc.

STATISTICAL ANALYSIS

Data are presented as means and standard deviations. The repeatability within each scan protocol was assessed using 3 repeated measurements. Interscan repeatability was evaluated by computing intraclass correlation coefficients (ICC) and 95% confidence intervals. Because measurements from both eyes of the same subject are likely to correlate, statistical methods are required that account for the fact that both eyes of an individual were included in the analysis. For this purpose, we used generalized estimating equations with robust standard errors (Huber-White sandwich variance estimator) to adjust for potential correlations. All tests were 2-sided, and a P value of less than .05 was considered

statistically significant. All statistical analyses were performed with commercially available software (Stata version 10.0; StataCorp, College Station, Texas, USA).

RESULTS

THIS PROSPECTIVE STUDY RECRUITED A TOTAL OF 60 EYES OF 30 subjects. No 3D scans could be obtained for 3 subjects for the following reasons: inability to obtain good quality scans because of small pupil (n = 1) and data lost because of device failure (n = 2). In addition, incomplete 3D data sets were obtained for some subjects, reducing the final data set used for analysis to 54 eyes of 27 subjects for the radial scan, 54 eyes of 27 subjects for the line scan, 50 eyes of 27 subjects for the 3D optic disc, and 49 eyes of 27 subjects for the 3D macula scan protocol. Therefore, complete data sets for all 4 scan protocols were obtained in 49 eyes. The mean (± standard deviation) age was 36.6 ± 10.4 years (range, 21 to 51 years) with 14 men and 13 women. Subjects were of white (n = 17), Hispanic (n = 4), Asian (n = 3), and other (n = 3) ancestry.

The mean retinal thicknesses were 307.9 ± 19.2 μm, 302.3 ± 15.5 μm, 267.0 ± 22.0 μm, and 252.7 ± 23.7 μm with the 3D macula scan, 3D optic disc scan, radial scan, and line scan protocol, respectively. The mean choroidal thicknesses were 219.3 ± 47.9 μm (3D macula), 177.2 ± 53.7 μm (3D optic disc), 94.0 ± 64.2 μm (radial), and 191.8 ± 61.8 μm (line). Data on retinal and choroidal thickness measurements as well as ICCs are summarized in Tables 1, 2, 3, and 4.

After quality control and exclusion of scans with artifacts (see below), the ICCs were higher for all scan protocols and ranged between 0.76 (line scan) and 0.89 (radial scan) for retinal thickness measurements and between 0.87 (radial scan) and 0.99 (3D optic disc scan) for choroidal thickness measurements. The ICC value for RNFL thickness varied from 0.73 (line scan) to 0.99 (radial scan; $P < .01$). For other individual retinal parameters, the ICCs ranged from 0.45 to 0.99. No statistically significant differences were found for repeatability of overall retinal and choroidal measurements between the different scan protocols.

IMAGE ARTIFACTS

Table 5 shows the number of scans available for analysis and reasons for exclusion by scan protocol. The most frequent image artifact was signal loss resulting from blinking. However, data on the frequency of blink artifact could be ascertained only from 3D protocols, because the radial and line protocols automatically exclude scans with signal loss resulting from blinking from the averaging process. Blinking artifacts covering less than 10% of the scan area occurred in 6.6% (10/151) of 3D optic disc and in 4.7% (7/149) of 3D macula scans. Figure 1 presents an example of a 3D macula scan with signal loss covering approximately 40% of the scan area. The effect on the B-scan obtained in the area of the signal loss is demonstrated on a 2D scan (Top center) and compared to a B-scan taken in an area unaffected by blinking (Bottom center). The effect of blink artifact on the integrity of choroidal segmentation lines can be visualized on the 3D scan (Right).

Segmentation failures occurred in a total of 15 scans. In 8 of these, there was a simultaneous failure of choroidal and retinal segmentation. Figure 2 shows a case in which the optic nerve

canal opening was not detected by the software and instead was transposed to an area with weaker signal strength corresponding to the boundaries of the chorioscleral interface. The segmentation failure was not present when the scan was repeated at the same location with a better signal-to-noise ratio (image quality, 138 vs 104 for first scan; Figure 2, Bottom). Other examples of segmentation failure are demonstrated in Figures 3 and 4.

Edge effects at the periphery of scans produced inaccurate segmentation in some eyes, but because these involved less than 25% of the scan area (Figure 5), these scans were included in the analysis. When scans with blink artifacts and segmentation failures were included in the analysis, ICC values for choroidal thickness measurements decreased to 0.92, 0.98, 0.80, and 0.91 for the 3D macula, 3D optic disc, radial, and line scans, respectively. For retinal thickness measurements, the ICCs dropped to 0.39, 0.49, 0.71, and 0.69, respectively.

Motion artifacts applied only to 3D scans and occurred in only 5 scans. Figure 6 demonstrates one such case in a 3D optic disc scan. A small area of signal loss resulting from blinking is seen in the superior part of the image. When scans with motion artifacts were excluded from the analysis, no statistically significant effect on the accuracy of the measurements was observed.

DISCUSSION

THE CURRENT STUDY EVALUATED THE REPEATABILITY OF retinal and choroidal thickness measurements using a prototype SS OCT instrument, the frequency of artifacts, and the impact of artifacts on measurement quality. We applied newly developed automated segmentation software to delineate retinal and choroidal structures and studied 4 SS OCT scan protocols. Our results demonstrate that automated measurements of retinal and choroidal thickness using SS OCT are highly repeatable; however, the presence of artifacts such as those caused by blinking can have a significant impact on the repeatability of measurements.

Before the introduction of the SS OCT, the use of SD OCT with the EDI protocol greatly enhanced the quality of in vivo imaging of the choroid.[14] In recent years, several investigators have used this technique to evaluate choroidal thickness in healthy subjects[14,29–35] and in patients with various retinal conditions[7,22,36] and glaucoma.[28,37] Although measuring the thickness of the choroid may be more challenging than measuring retinal thickness, because of high local variability of the choroid, the comparison of choroidal thickness measurements generally yield good agreement between studies. There are, however, some notable differences between studies, with a large range in mean subfoveal measurements from as large as 372.2 μm to as small as 191.5 μm.[21,29] In addition to differences in the study population, discrepancies among studies can be explained by several factors. First, in the absence of automated demarcation of the choroidal boundaries, most investigators have used single location measurements for determination of choroidal thickness. Point-to-point measurements of the choroid, however, are a problematic method not only because of operator bias, but also because of the highly variable choroidal anatomic features. Unlike the retina, the choroid is a highly vascularized structure with significant diurnal fluctuations in thickness.[29] The effect of the circadian cycle therefore may account

for some of the reported differences in choroidal thickness. Despite these factors, Mwanza and associates demonstrated that high repeatability of manual measurements could be obtained with ICC values of 0.99 for foveal, nasal, and temporal choroidal thicknesses.[38]

Several recent SD OCT studies applied more objective methods for choroidal thickness measurements. Chhablani and associates used a novel method based on modification of the EDI SD OCT retinal segmentation software (Spectralis; Heidelberg Engineering, Heidelberg, Germany) to demarcate the choroid.[22] They reported mean foveal choroidal thicknesses of 264.15 and 263.83 μm, measured by 2 independent graders, with high intergrader agreement ($\rho = 0.996$). Shin and associates proposed a similar approach and created an Early Treatment Diabetic Retinopathy Study-style topographic map of choroidal thickness by modifying the 6 radial scan protocol used with SD OCT (3D OCT-2000; Topcon, Tokyo, Japan).[35] These methods, however, are time consuming (167 seconds per eye in the Shin and associates study) and not fully automated because they still depend on manual adjustment of choroidal boundaries.

SS OCT instruments use a longer wavelength than SD OCT and in theory are better placed to visualize deeper ocular structures. In contrast to the EDI technique, in which resolution of the retina structures is reduced as a trade-off to better visualization of the choroid,[14] SS OCT is capable of imaging the retina and choroid equally well. Esmaeelpour and associates also suggested that SS OCT may provide superior visualization of the posterior pole in patients with media opacities.[39]

The limitation of manual measurements was demonstrated by Ikuno and associates, who reported moderate ICCs of 0.6 to 0.8 using both EDI SD OCT and SS OCT.[23] Using the Early Treatment Diabetic Retinopathy Study map technique on SS OCT scans, Hirata and associates obtained significantly higher ICCs of 0.95 and 0.98 for reproducibility of choroidal thickness measurements of 2 graders.[21] The current study used automated segmentation of the choroid to obtain operator-independent and objective measurements of thickness and volume with an SS OCT instrument.

Currently, there are no guidelines concerning the use of specific scan protocols in a clinical setting. Therefore, we evaluated the repeatability of retinal and choroidal thickness measurements with 4 different scan protocols that may be provided in future commercial models. With ICCs ranging from 0.87 to 0.99, all scan protocols were able to obtain thickness measurements with a high level of repeatability. Interestingly, in the current study, repeatability of retinal thickness measurements was lower (ICC, 0.76 to 0.89) than that of choroidal measurements (ICC, 0.87 to 0.99) in 3 of 4 scan protocols. Similar results were reported in another study, in which manual measurements were obtained from both SD OCT and SS OCT instruments.[23] A possible explanation may be that the longer wavelength of the SS OCT device and the use of the choroidal reference position in the current study may have affected retinal thickness measurements adversely.

In the current study, between 3% and 9% of scans (according to scan protocol) were excluded from the analysis because of the presence of artifacts, the most common of which was signal loss resulting from eye blinks. During signal loss, measurement errors resulting

from the continued presence of segmentation lines occur. Interestingly, these arbitrary measurements seem to deviate significantly more from the actual retinal thickness measurements than from choroidal ones when the signal returns (Figure 1). This difference may be the result of the differences in the smoothing process that is performed as a postprocessing operation in which boundary locations in relation to a reference are smoothed across frames. This can result in a situation where automatically segmented boundaries may show a rough retinal form in noise frames that are adjacent to or nearly adjacent to valid frames. The smoothing processing is somewhat different for the retinal boundaries compared with choroidal boundaries. This may explain why overall ICCs for choroidal thickness values change only slightly after exclusion of artifacts (from 0.98 to 0.99 for 3D optic disc scans and from 0.92 to 0.95 for 3D macula scans), whereas those for retinal values improve dramatically (from 0.39 to 0.88 and from 0.49 to 0.83, respectively). The impact of this artifact constitutes a weakness of 3D scans, which do not automatically exclude scans with signal loss from processing (as do the other 2 scan protocols). Therefore, its presence and impact on measurements warrants close inspection during the quality control process.

Segmentation failures occurred relatively infrequently (12 scans) and their impact on overall repeatability was relatively small. For instance, for the line scan protocol, overall ICCs for retinal and choroidal thicknesses were reduced from 0.76 to 0.69 and from 0.93 to 0.91, respectively, when scans with this artifact were included. Figure 4 demonstrates how a posterior vitreous detachment can lead to a misidentification of the inner retina in some scans. However, the overall effect on measurements was minimal, and these scans were included in the analysis. Motion artifacts occurred rarely and did not affect overall measurement repeatability, as demonstrated in Figure 6.

Previous studies have demonstrated a lower frequency of artifacts in SD OCT compared with the older time-domain OCT instruments.[27,40,41] More recently, Maul and associates performed an EDI OCT study to evaluate factors affecting choroidal thickness in glaucoma patients.[37] They divided scans into good, fair, and poor quality based on whether the chorioscleral interface was well delineated and thinner than the retinal pigment epithelium, whether it was thicker than the retinal pigment epithelium, or whether no chorioscleral interface boundary was visible. They found that poor-quality images on average had a thicker choroid than fair- and good-quality images. No further information about the presence of image artifacts was provided.

This study has some potential limitations. At present, only prototype SS OCTs have been investigated. The first commercial instruments only have recently become available. It is not known to what extent findings from investigations of prototype instruments will be transposable to the commercial instruments. In the current study, subjects' eyes were not dilated to reflect a real-life situation. Small pupils, however, may have had an adverse effected the quality of scans, although previous studies evaluating SD OCT devices have not found such an effect.[42,43] Last, this study examined healthy eyes of young subjects, and therefore, the findings may not be generalizable to elderly patients with ocular disease. It was shown previously that specific types of retinal pathologic features were apt to elicit specific types of artifacts on SD OCT scans.[40]

In conclusion, although all SS OCT scan protocols examined in this study revealed high repeatability, we found that signal loss resulting from blinking is a common artifact resulting in substantial measurement errors. Despite the relatively low frequency of other artifacts with SS OCT imaging in this group of young healthy subjects, recognizing their presence and adverse influence on measurements is important and may influence clinical decisions.

Supplementary Material

Refer to Web version on PubMed Central for supplementary material.

Acknowledgments

Dr Mansouri has received research and financial support from Sensimed AG; Dr Medeiros has received research and financial support from Carl Zeiss Meditec, Inc, Pfizer, Inc, and Reichert, Inc; and Dr Weinreb has received research and financial support from Carl Zeiss Meditec, Inc, Heidelberg Engineering, GmbH, Optovue, Inc, Topcon Medical Systems, Inc, and Nidek. Supported by National Eye Institute Grant R01021818 (F.A.M.), Bethesda, Maryland; the Velux Foundation, Zurich, Switzerland (K.M.); the Swiss Foundation for the Prevention of Blindness, Zurich, Switzerland (K.M.); and by an unrestricted grant from Research to Prevent Blindness, Inc, New York, New York. Involved in Design of study (K.M.); Conduct of study (A.J.T., K.M., N.M.); Statistical expertise (K.M., F.A.M.); Provision of materials, subjects, or resources (K.M., R.N.W.); Writing article (K.M.); and Critical revision of article and final approval (K.M., F.A.M., A.J.T., N.M., R.N.W.).

Biography

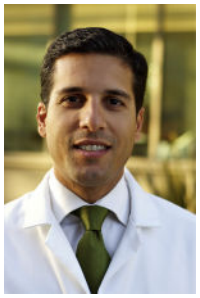

Kaweh Mansouri, MD, MPH, is a consultant ophthalmologist at the Glaucoma sector, Department of Ophthalmology, University of Geneva. He was previously a senior fellow at the Hamilton Glaucoma Center, University of California at San Diego, California. He completed his residency in ophthalmology at the Jules Gonin Eye Hospital, University of Lausanne, Switzerland. His research interests include 24-hour intraocular pressure monitoring, imaging and surgical innovations in glaucoma.

References

1. Swanson EA, Izatt JA, Hee MR, et al. In vivo retinal imaging by optical coherence tomography. Opt Lett. 1993; 18(21):1864–1866. [PubMed: 19829430]
2. Mansouri K, Leite MT, Medeiros FA, Leung CK, Weinreb RN. Assessment of rates of structural change in glaucoma using imaging technologies. Eye. 2011; 25(3):269–277. [PubMed: 21212798]
3. Leitgeb R, Hitzenberger C, Fercher A. Performance of fourier domain vs. time domain optical coherence tomography. Opt Express. 2003; 11(8):889–894. [PubMed: 19461802]
4. Gloesmann M, Hermann B, Schubert C, Sattmann H, Ahnelt PK, Drexler W. Histologic correlation of pig retina radial stratification with ultrahigh-resolution optical coherence tomography. Invest Ophthalmol Vis Sci. 2003; 44(4):1696–1703. [PubMed: 12657611]

5. Mansouri K, Liu JH, Tafreshi A, Medeiros FA, Weinreb RN. Positional independence of optic nerve head and retinal nerve fiber layer thickness measurements with spectral-domain optical coherence tomography. Am J Ophthalmol. 2012; 154(4):712–721. [PubMed: 22818801]
6. Spaide RF. Age-related choroidal atrophy. Am J Ophthalmol. 2009; 147(5):801–810. [PubMed: 19232561]
7. Imamura Y, Fujiwara T, Margolis R, Spaide RF. Enhanced depth imaging optical coherence tomography of the choroid in central serous chorioretinopathy. Retina. 2009; 29(10):1469–1473. [PubMed: 19898183]
8. Kubota T, Jonas JB, Naumann GO. Decreased choroidal thickness in eyes with secondary angle closure glaucoma. An aetiological factor for deep retinal changes in glaucoma? Br J Ophthalmol. 1993; 77(7):430–432. [PubMed: 8343472]
9. Yin ZQ, Vaegan Millar TJ, Beaumont P, Sarks S. Widespread choroidal insufficiency in primary open-angle glaucoma. J Glaucoma. 1997; 6(1):23–32. [PubMed: 9075077]
10. Hirooka K, Fujiwara A, Shiragami C, Baba T, Shiraga F. Relationship between progression of visual field damage and choroidal thickness in eyes with normal-tension glaucoma. Clin Experiment Ophthalmol. 2012; 40(6):576–582. [PubMed: 22300430]
11. Haefliger IO, Flammer J, Luscher TF. Heterogeneity of endothelium-dependent regulation in ophthalmic and ciliary arteries. Invest Ophthalmol Vis Sci. 1993; 34(5):1722–1730. [PubMed: 8473112]
12. Hayreh SS. Blood supply of the optic nerve head and its role in optic atrophy, glaucoma, and oedema of the optic disc. Br J Ophthalmol. 1969; 53(11):721–748. [PubMed: 4982590]
13. Hung LF, Wallman J, Smith EL 3rd. Vision-dependent changes in the choroidal thickness of macaque monkeys. Invest Ophthalmol Vis Sci. 2000; 41(6):1259–1269. [PubMed: 10798639]
14. Spaide RF, Koizumi H, Pozzoni MC. Enhanced depth imaging spectral-domain optical coherence tomography. Am J Ophthalmol. 2008; 146(4):496–500. [PubMed: 18639219]
15. Lee EJ, Kim TW, Weinreb RN, et al. Three-dimensional evaluation of the lamina cribrosa using spectral-domain optical coherence tomography in glaucoma. Invest Ophthalmol Vis Sci. 2012; 53(1):198–204. [PubMed: 22167102]
16. Ikuno Y, Kawaguchi K, Nouchi T, Yasuno Y. Choroidal thickness in healthy Japanese subjects. Invest Ophthalmol Vis Sci. 2010; 51(4):2173–2176. [PubMed: 19892874]
17. Mansouri K, Medeiros FA, Marchase N, Tatham AJ, Auerbach D, Weinreb RN. Assessment of choroidal thickness and volume during the water drinking test by swept-source optical coherence tomography. Ophthalmology. 2013; 120(12):2508–2516. [PubMed: 24021895]
18. Mansouri K, Nuyen B, N Weinreb R. Improved visualization of deep ocular structures in glaucoma using high penetration optical coherence tomography. Expert Rev Med Devices. 2013; 10(5):621–628. [PubMed: 23972075]
19. Jirarattanasopa P, Ooto S, Tsujikawa A, et al. Assessment of macular choroidal thickness by optical coherence tomography and angiographic changes in central serous chorioretinopathy. Ophthalmology. 2012; 119(8):1666–1678. [PubMed: 22521082]
20. Usui S, Ikuno Y, Miki A, Matsushita K, Yasuno Y, Nishida K. Evaluation of the choroidal thickness using high-penetration optical coherence tomography with long wavelength in highly myopic normal-tension glaucoma. Am J Ophthalmol. 2012; 153(1):10–16.e11. [PubMed: 21864827]
21. Hirata M, Tsujikawa A, Matsumoto A, et al. Macular choroidal thickness and volume in normal subjects measured by swept-source optical coherence tomography. Invest Ophthalmol Vis Sci. 2011; 52(8):4971–4978. [PubMed: 21622704]
22. Chhablani J, Barteselli G, Wang H, et al. Repeatability and reproducibility of manual choroidal volume measurements using enhanced depth imaging optical coherence tomography. Invest Ophthalmol Vis Sci. 2012; 53(4):2274–2280. [PubMed: 22427584]
23. Ikuno Y, Maruko I, Yasuno Y, et al. Reproducibility of retinal and choroidal thickness measurements in enhanced depth imaging and high-penetration optical coherence tomography. Invest Ophthalmol Vis Sci. 2011; 52(8):5536–5540. [PubMed: 21508114]

24. Usui S, Ikuno Y, Akiba M, et al. Circadian changes in subfoveal choroidal thickness and the relationship with circulatory factors in healthy subjects. Invest Ophthalmol Vis Sci. 2012; 53(4): 2300–2307. [PubMed: 22427554]
25. Agawa T, Miura M, Ikuno Y, et al. Choroidal thickness measurement in healthy Japanese subjects by three-dimensional high-penetration optical coherence tomography. Graefes Arch Clin Exp Ophthalmol. 2011; 249(10):1485–1492. [PubMed: 21556938]
26. Yasuno Y, Hong Y, Makita S, et al. In vivo high-contrast imaging of deep posterior eye by 1-microm swept source optical coherence tomography and scattering optical coherence angiography. Opt Express. 2007; 15(10):6121–6139. [PubMed: 19546917]
27. Ho J, Sull AC, Vuong LN, et al. Assessment of artifacts and reproducibility across spectral- and time-domain optical coherence tomography devices. Ophthalmology. 2009; 116(10):1960–1970. [PubMed: 19592109]
28. Roberts KF, Artes PH, O'Leary N, et al. Peripapillary choroidal thickness in healthy controls and patients with focal, diffuse, and sclerotic glaucomatous optic disc damage. Arch Ophthalmol. 2012; 130(8):980–986. [PubMed: 22491392]
29. Tan CS, Ouyang Y, Ruiz H, Sadda SR. Diurnal variation of choroidal thickness in normal, healthy subjects measured by spectral domain optical coherence tomography. Invest Ophthalmol Vis Sci. 2012; 53(1):261–266. [PubMed: 22167095]
30. Ding X, Li J, Zeng J, et al. Choroidal thickness in healthy Chinese subjects. Invest Ophthalmol Vis Sci. 2011; 52(13):9555–9560. [PubMed: 22058342]
31. Chen FK, Yeoh J, Rahman W, Patel PJ, Tufail A, Da Cruz L. Topographic variation and interocular symmetry of macular choroidal thickness using enhanced depth imaging optical coherence tomography. Invest Ophthalmol Vis Sci. 2012; 53(2):975–985. [PubMed: 22232433]
32. Rahman W, Chen FK, Yeoh J, Patel P, Tufail A, Da Cruz L. Repeatability of manual subfoveal choroidal thickness measurements in healthy subjects using the technique of enhanced depth imaging optical coherence tomography. Invest Ophthalmol Vis Sci. 2011; 52(5):2267–2271. [PubMed: 21087970]
33. Branchini L, Regatieri CV, Flores-Moreno I, Baumann B, Fujimoto JG, Duker JS. Reproducibility of choroidal thick ness measurements across three spectral domain optical coherence tomography systems. Ophthalmology. 2012; 119(1):119–123. [PubMed: 21943786]
34. Yamashita T, Shirasawa M, Arimura N, Terasaki H, Sakamoto T. Repeatability and reproducibility of subfoveal choroidal thickness in normal eyes of Japanese using different SD-OCT devices. Invest Ophthalmol Vis Sci. 2012; 53(3):1102–1107. [PubMed: 22247474]
35. Shin JW, Shin YU, Lee BR. Choroidal thickness and volume mapping by a six radial scan protocol on spectral-domain optical coherence tomography. Ophthalmology. 2012; 119(5):1017–1023. [PubMed: 22281089]
36. Maruko I, Iida T, Sugano Y, Ojima A, Sekiryu T. Subfoveal choroidal thickness in fellow eyes of patients with central serous chorioretinopathy. Retina. 2011; 31(8):1603–1608. [PubMed: 21487334]
37. Maul EA, Friedman DS, Chang DS, et al. Choroidal thickness measured by spectral domain optical coherence tomography: factors affecting thickness in glaucoma patients. Ophthalmology. 2011; 118(8):1571–1579. [PubMed: 21492939]
38. Mwanza JC, Hochberg JT, Banitt MR, Feuer WJ, Budenz DL. Lack of association between glaucoma and macular choroidal thickness measured with enhanced depth-imaging optical coherence tomography. Invest Ophthalmol Vis Sci. 2011; 52(6):3430–3435. [PubMed: 21357398]
39. Esmaeelpour M, Povazay B, Hermann B, et al. Three-dimensional 1060-nm OCT: choroidal thickness maps in normal subjects and improved posterior segment visualization in cataract patients. Invest Ophthalmol Vis Sci. 2010; 51(10):5260–5266. [PubMed: 20445110]
40. Ray R, Stinnett SS, Jaffe GJ. Evaluation of image artifact produced by optical coherence tomography of retinal pathology. Am J Ophthalmol. 2005; 139(1):18–29. [PubMed: 15652824]
41. Mylonas G, Ahlers C, Malamos P, et al. Comparison of retinal thickness measurements and segmentation performance of four different spectral and time domain OCT devices in neovascular age-related macular degeneration. Br J Ophthalmol. 2009; 93(11):1453–1460. [PubMed: 19520692]

42. Medina FJ, Callen CI, Rebolleda G, Munoz-Negrete FJ, Callen MJ, del Valle FG. Use of nonmydriatic spectral-domain optical coherence tomography for diagnosing diabetic macular edema. Am J Ophthalmol. 2012; 153(3):536–543.e1. [PubMed: 21996307]

43. Massa GC, Vidotti VG, Cremasco F, Lupinacci AP, Costa VP. Influence of pupil dilation on retinal nerve fibre layer measurements with spectral domain OCT. Eye. 2010; 24(9):1498–1502. [PubMed: 20508653]

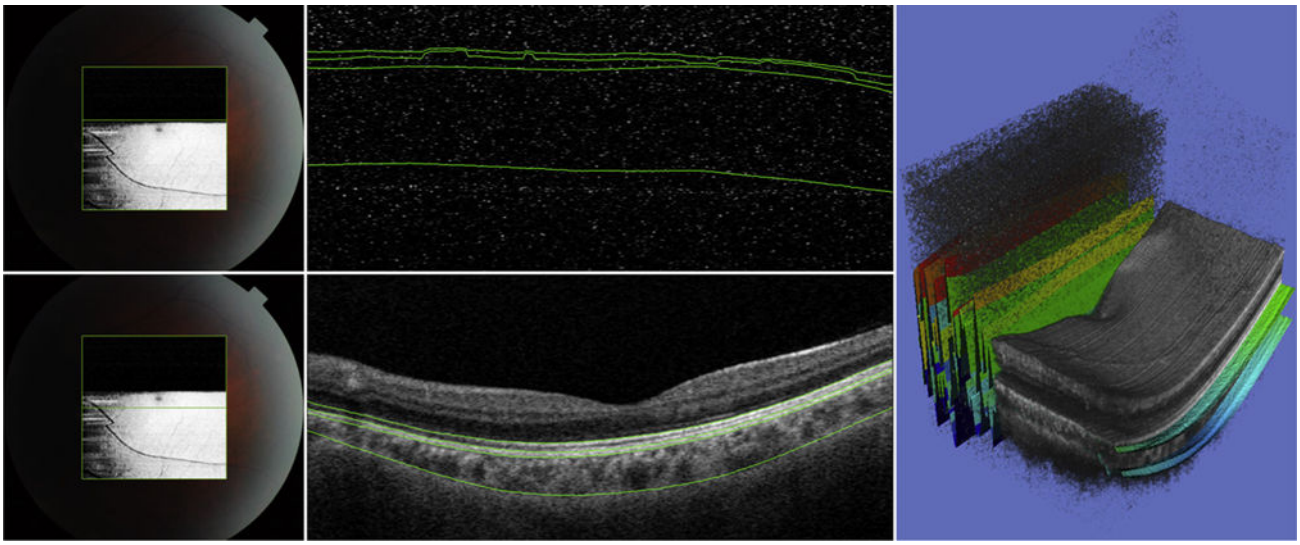

FIGURE 1.

Retinal and choroidal thickness by swept-source optical coherence tomography: demonstration of blink artifact with the 3-dimensional (3D) macula scan protocol. (Top left) Fundus image demonstrating area of the 3D scan (green square). The blackened area in the superior part of the image corresponds to signal loss resulting from blinking. The green line indicates the area of the B-scan. (Top center) Corresponding B-scan. Note the continued use of retinal and choroidal segmentation lines despite absence of signal. (Bottom left) Fundus image demonstrating position of measurement outside the area of signal loss (green line). (Bottom center) Corresponding B-scan with correct segmentation of choroidal boundaries and outer retinal layers. (Right) Resulting 3D macula tomograph illustrating continued application of segmentation lines despite absence of signal in the superior macular region. In the intact inferior region, accurate segmentation of choroidal borders can be visualized (color lines).

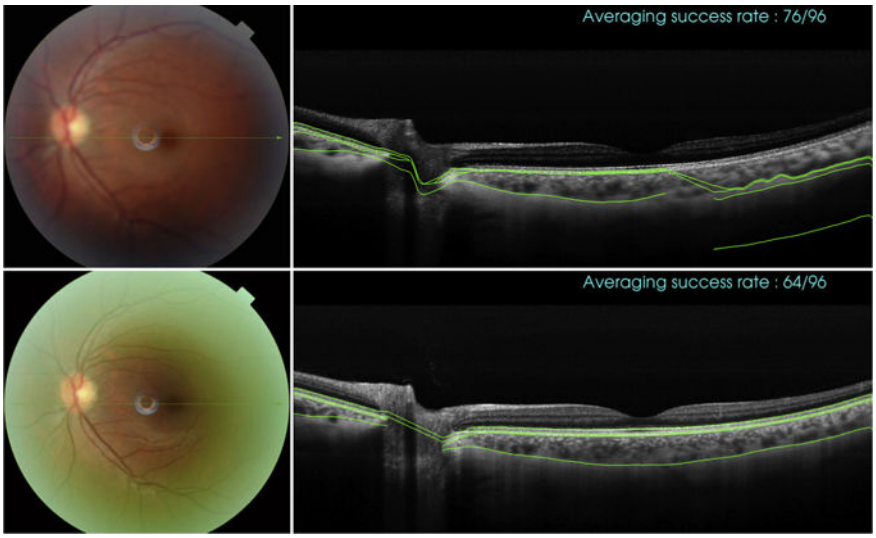

FIGURE 2.

Example of a swept-source optical coherence tomography scan demonstrating segmentation failure on a 12-mm horizontal line scan. (Top left) Fundus image demonstrating area and orientation of the line scan (green line, temporal scan direction). (Top right) Outer choroid misidentification: in approximately 50% of the scan area, the segmentation line does not follow the retinal pigment epithelium (RPE) with subsequent displacement of chorioscleral interface (CSI) segmentation (indicated by dashed line). (Bottom left) Fundus image from repeat scan obtained at the same location (green line, temporal scan direction). (Bottom right) Correct identification of RPE and CSI.

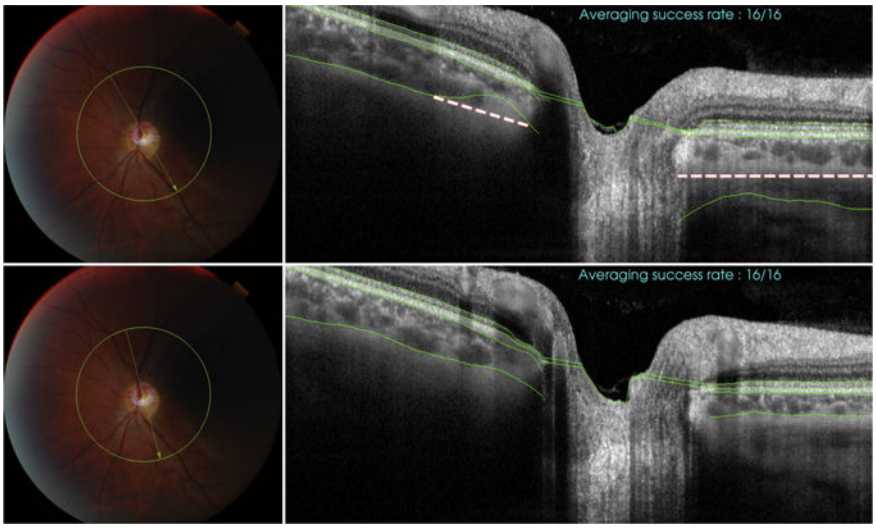

FIGURE 3.

Demonstration of segmentation failure on a 12-line radial scan protocol using swept-source optical coherence tomography (SS OCT). (Top left) Fundus image demonstrating plane and orientation of the line scan (green line). (Top right) The SS OCT software failed to recognize a less well-demarcated posterior choroidal surface and instead identified the posterior scleral interface as chorioscleral interface (CSI) in approximately 75% of the scan area. (Bottom left) Fundus image of the adjacent clock hour scan of the same eye. (Bottom right) The CSI was identified correctly by the segmentation software.

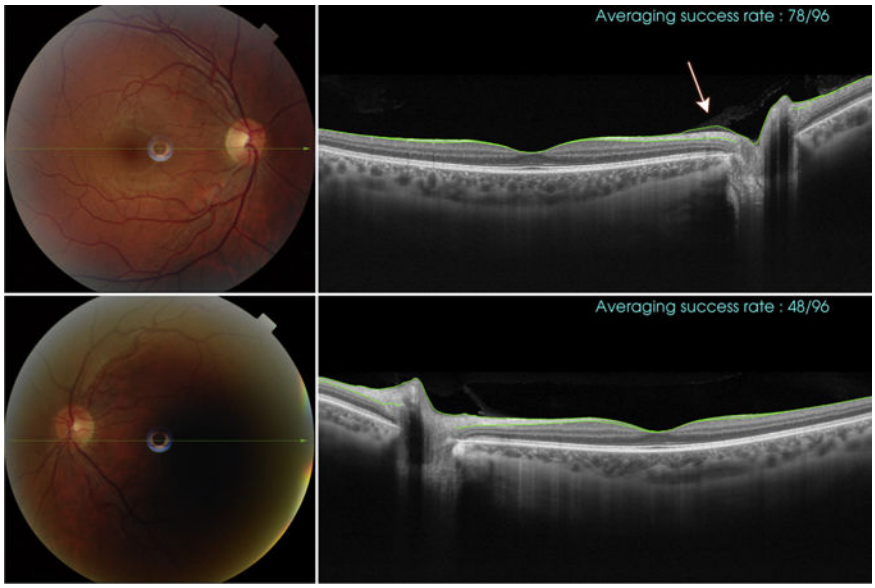

FIGURE 4.

Demonstration of retinal segmentation failure with the 12-mm line scan protocol using swept-source optical coherence tomography (SS OCT). (Top left) Fundus image demonstrating plane and orientation of the line scan (green line). (Top right) The SS OCT software misidentified a posterior vitreous detachment (arrow) as the inner retinal boundary. (Bottom left) Fundus image of the contralateral eye of the same patient. (Bottom right) Inner retina was identified correctly by the segmentation software, despite presence of posterior vitreous detachment.

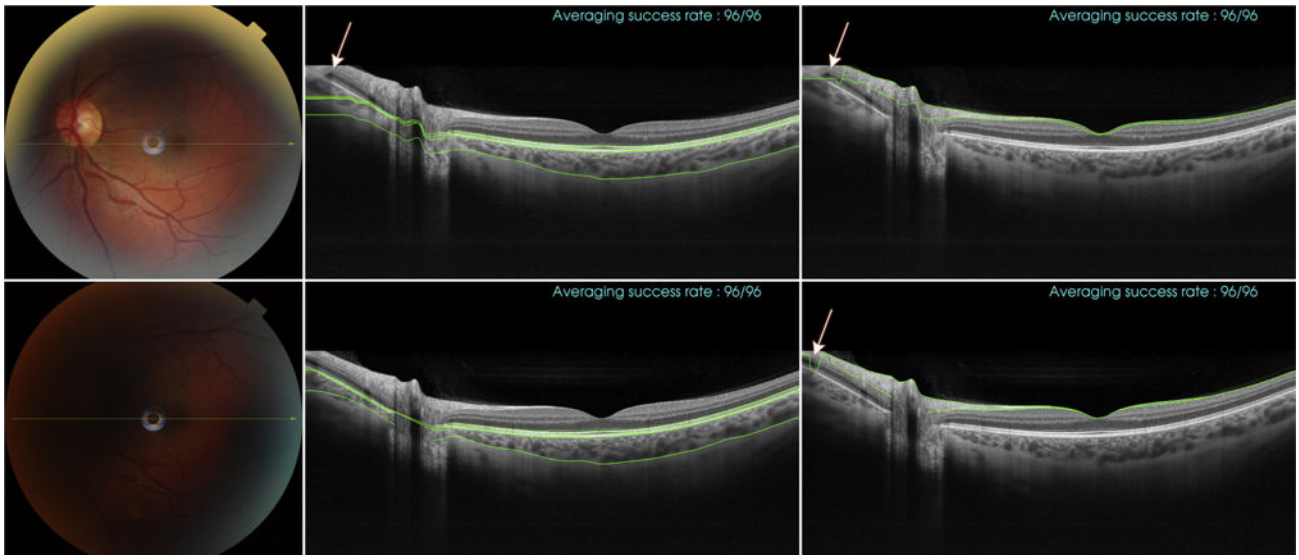

FIGURE 5.

Demonstration of segmentation failure resulting from scan edge effect with the 12-mm line scan protocol of swept-source optical coherence tomography. (Top left) Fundus image demonstrating plane and orientation of the line scan (green line). (Top center) Incorrect identification of inner and outer choroidal limits at the nasal edge of the scan (arrow). (Top right) The retinal segmentation lines correctly end close to the edge of the scan (arrow). (Bottom) Correct identification of choroidal and retinal segments is achieved in the second scan of the same eye.

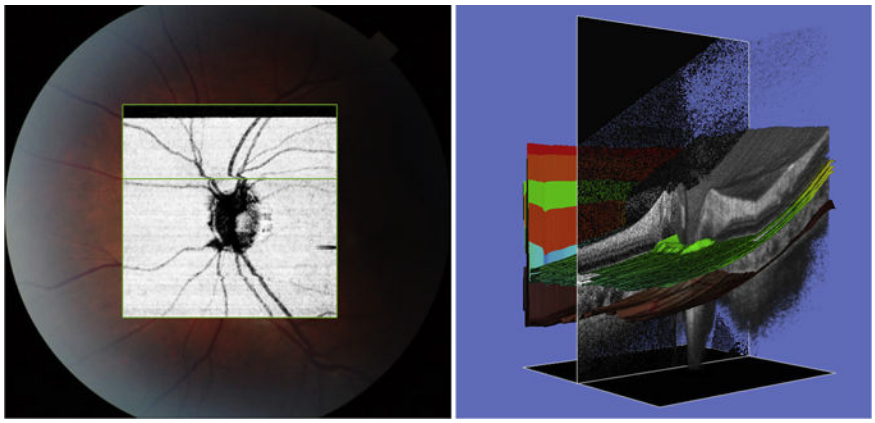

FIGURE 6.

Demonstration of simultaneous presence of motion and blink artifact on the 3-dimensional (3D) optic disc tomograph. (Left) Fundus image with en face projection demonstrating presence of a motion artifact (kinking of vessels, best visible on superior vessel arcade) on a 3D scan. Signal loss resulting from a blink covering approximately 10% of the scan area can be seen at the superior edge of the image (black area). (Right) Although the effect of blink artifact on segmentation is clearly visible (superior part of 3D tomograph), there is no impact of the motion artifact on outer retinal and choroidal segmentation lines. The cross-sectional shadowgram (ie, perpendicular translucent black window) corresponds to the green line on the fundus image and highlights the area of maximal vessel displacement.

TABLE 1

Three-Dimensional Macula Scan Protocol of Swept-Source Optical Coherence Tomography: Average Retinal and Choroidal Thickness and Volume in 27 Subjects (49 Eyes) during 3 Consecutive Measurements after Exclusion of Image Artifacts

Parameters	Overall Mean ± SD	ICC (95% CI)
RNFL thickness (μm)	50.2 ± 10.7	0.92 (0.90 to 0.95)
GCL thickness (μm)	37.1 ± 3.4	0.79 (0.70 to 0.86)
GCC thickness (μm)	31.4 ± 3.1	0.78 (0.70 to 0.84)
OPL thickness (μm)	28.8 ± 2.0	0.92 (0.89 to 0.94)
ELM thickness (μm)	75.4 ± 5.3	0.99 (0.98 to 0.99)
IS/OS junction thickness (μm)	20.8 ± 1.4	0.82 (0.75 to 0.87)
RPE thickness (μm)	40.1 ± 3.5	0.95 (0.94 to 0.96)
BM thickness (μm)	24.1 ± 2.8	0.52 (0.38 to 0.69)
Retina thickness (μm)	307.9 ± 19.2	0.88 (0.85 to 0.91)
Choroidal thickness (μm)	219.3 ± 47.9	0.95 (0.93 to 0.96)
Choroidal volume (mm^3)	7.87 ± 1.72	0.95 (0.93 to 0.96)

BM = Bruch membrane; CI = confidence interval; ELM = external limiting membrane; GCC = ganglion cell complex (including the internal plexiform layer [IPL] and the internal nuclear layer); GCL = ganglion cell layer (GCL/IPL); ICC = intraclass correlation coefficient; ISOS = inner segment/outer segment; OPL = outer plexiform layer; RNFL = retinal nerve fiber layer; RPE = retinal pigment epithelium (OS/RPE); SD = standard deviation.

TABLE 2

Three-Dimensional Optic Disc Scan Protocol of Swept-Source Optical Coherence Tomography: Average Retinal and Choroidal Thickness and Volume in 27 Subjects (50 Eyes) during 3 Consecutive Measurements after Exclusion of Image Artifacts

Parameters	Overall Mean ± SD	ICC (95% CI)
RNFL thickness (μm)	87.6 ± 7.8	0.87 (0.80 to 0.90)
GCL thickness (μm)	22.6 ± 2.0	0.67 (0.58 to 0.77)
GCC thickness (μm)	23.0 ± 2.8	0.90 (0.82 to 0.87)
OPL thickness (μm)	23.0 ± 2.8	0.86 (0.80 to 0.89)
ELM thickness (μm)	65.2 ± 5.2	0.92 (0.89 to 0.94)
IS/OS junction thickness (μm)	19.7 ± 2.4	0.82 (0.73 to 0.88)
RPE thickness (μm)	36.1 ± 6.6	0.93 (0.91 to 0.95)
BM thickness (μm)	24.7 ± 1.9	0.93 (0.90 to 0.95)
All retina thickness (μm)	302.3 ± 15.5	0.84 (0.78 to 0.87)
Choroidal thickness (μm)	177.2 ± 53.7	0.99 (0.98 to 0.99)
Choroidal volume (mm^3)	6.03 ± 1.85	0.99 (0.98 to 0.99)

BM = Bruch membrane; CI = confidence interval; ELM = external limiting membrane; GCC = ganglion cell complex (including the internal plexiform layer [IPL] and the internal nuclear layer); GCL = ganglion cell layer (GCL/IPL); ICC = intra-class correlation coefficient; IS/OS = inner segment/outer segment; OPL = outer plexiform layer; RNFL = retinal nerve fiber layer; RPE = retinal pigment epithelium (OS/RPE); SD = standard deviation.

TABLE 3

Radial Scan Protocol of Swept-Source Optical Coherence Tomography; Average Retinal and Choroidal Thickness in 27 Subjects (54 Eyes) during 3 Consecutive Measurements

Parameters	Overall Mean ± SD	ICC (95% CI)
RNFL thickness (μm)	56.2 ± 35.4	0.99 (0.98 to 1.0)
GCL thickness (μm)	42.0 ± 30.3	0.99 (0.98 to 1.0)
GCC thickness (μm)	19.3 ± 2.7	0.71 (0.60.0.79)
OPL thickness (μm)	19.3 ± 2.7	0.45 (0.31 to 0.64)
ELM thickness (μm)	39.4 ± 16.4	0.98 (0.97 to 0.1.0)
IS/OS junction thickness (μm)	29.1 ± 18.6	0.99 (0.98 to 1.0)
RPE thickness (μm)	23.5 ± 6.6	0.97 (0.96 to 0.99)
BM thickness (μm)	23.8 ± 4.5	0.88 (0.83 to 0.92)
All retina thickness (μm)	252.7 ± 23.7	0.89 (0.85 to 0.92)
Choroidal thickness (μm)	94.2 ± 64.2	0.87 (0.83 to 0.91)

BM = Bruch membrane; CI = confidence interval; ELM = external limiting membrane; GCC = ganglion cell complex (including the internal plexiform layer [IPL] and the internal nuclear layer); GCL = ganglion cell layer (GCL/IPL); ICC = intraclass correlation coefficient; IS/OS = inner segment/outer segment; OPL = outer plexiform layer; RNFL = retinal nerve fiber layer; RPE = retinal pigment epithelium (OS/RPE); SD = standard deviation.

TABLE 4

Twelve-Millimeter Line Scan Protocol of Swept-Source Optical Coherence Tomography: Average Retinal and Choroidal Thickness in 27 Subjects (54 Eyes) during 3 Consecutive Measurements

Parameters	Overall Mean ± SD	ICC (95% CI)
RNFL thickness (μm)	32.6 ± 10.8	0.73 (0.62 to 0.91)
GCL thickness (μm)	32.3 ± 4.6	0.56 (0.39 to 0.76)
GCC thickness (μm)	30.1 ± 4.7	0.55 (0.38 to 0.72)
OPL thickness (μm)	23.8 ± 2.3	0.67 (0.53 to 0.79)
ELM thickness (μm)	71.1 ± 6.0	0.81 (0.73 to 0.87)
IS/OS junction thickness (μm)	18.9 ± 2.4	0.58 (0.41 to 0.75)
RPE thickness (μm)	34.1 ± 4.3	0.76 (0.66 to 0.84)
BM thickness (μm)	24.1 ± 3.5	0.54 (0.38 to 0.69)
All retina thickness (μm)	268.5 ± 22.5	0.76 (0.64 to 0.86)
Choroidal thickness (μm)	195.8 ± 61.9	0.93 (0.91 to 0.95)

BM = Bruch membrane; CI = confidence interval; ELM = external limiting membrane; GCC = ganglion cell complex (including the internal plexiform layer [IPL] and the internal nuclear layer); GCL = ganglion cell layer (GCL/IPL); ICC = intraclass correlation coefficient; IS/OS = inner segment/outer segment; OPL = outer plexiform layer; RNFL = retinal nerve fiber layer; RPE = retinal pigment epithelium (OS/RPE); SD = standard deviation.

TABLE 5

Retinal and Choroidal Thickness by Swept-Source Optical Coherence Tomography: Availability of Scans and Reasons for Exclusion (54 Eyes of 27 Subjects)

Scan Protocol	Scans Acquired/Scans Retained (n)[a]	Scans Excluded, n (%)	Reasons for Exclusion (n)[b]
3D macula scan	162/149	14(9)	Blinks (14), motion artifact (3), segmentation failure (1)
3D optic disc scan	162/151	11(7)	Blinks (10), motion artifact (2), segmentation failure (2)
Radial scan	162/161	7(4)	Segmentation failure (7)
Line scan	162/162	5(3)	Segmentation failure (5)

3D = 3-dimensional.

[a] Only scans with a minimum 50% averaging success were saved during the acquisition process.

[b] Multiple simultaneous artifacts were allowed to coexist.